DEVELOPMENTAL BIOLOGY

Imaging and tracing the pattern of adult ovarian angiogenesis implies a strategy against female reproductive aging

Xueqiang Xu[1], Lu Mu[1], Lingyu Li[1], Jing Liang[1], Shuo Zhang[1], Longzhong Jia[1], Xuebing Yang[1], Yanli Dai[1], Jiawei Zhang[1], Yibo Wang[1], Shudong Niu[1], Guoliang Xia[1], Yunlong Yang[2], Yan Zhang[1], Yihai Cao[3], Hua Zhang[1]*

Robust angiogenesis is continuously active in ovaries to remodel the ovary-body connections in mammals, but understanding of this unique process remains elusive. Here, we performed high-resolution, three-dimensional ovarian vascular imaging and traced the pattern of ovarian angiogenesis and vascular development in the long term. We found that angiogenesis was mainly active on ovarian follicles and corpus luteum and that robust angiogenesis constructs independent but temporary vascular networks for each follicle. Based on the pattern of ovarian angiogenesis, we designed an angiogenesis-blocking strategy by axitinib administration to young females, and we found that the temporary suppression of angiogenesis paused ovarian development and kept the ovarian reserve in the long term, leading to postponed ovarian senescence and an extension of the female reproductive life span. Together, by uncovering the detailed model of physiological ovarian angiogenesis, our experiments suggest a potential approach to delay female reproductive aging through the manipulation of angiogenesis.

INTRODUCTION

As the sexual gland of female mammals, the ovaries produce mature eggs and maintain the normal female endocrine. During the period of female reproductive activity, the adult ovaries present cyclic development with the recruitment and regression of ovarian follicles (*1*). This cyclic development makes the ovaries one of the few organs with active adult angiogenesis and vascular remodeling under physiological conditions (*2*–*4*). Although angiogenesis-related remodeling and the reconstitution of adult ovarian blood vessels are crucial for the regulation of female reproduction (*5*), a detailed model of this unique process has not been well described.

Angiogenesis is the process of growing new blood vessels from the original vascular structure (*6*). As a unique and highly programmed process, angiogenesis is mainly active in organogenesis during embryo development, in pathological conditions such as wound healing (*7*) and tumorigenesis (*8*, *9*), and in adult female reproductive organs under physiological conditions (*10*). Since the process of angiogenesis is essential for tumorigenesis (*6*, *11*), great progress has been made in the field of angiogenesis signaling and regulation and in the development of antiangiogenic drugs in the past 20 years (*12*–*14*). Several drugs that specifically block the vascular endothelial growth factor (VEGF) signaling pathway (*15*), such as axitinib (Axi) (*16*, *17*), have been widely applied to suppress the progression of tumor angiogenesis in clinical practice (*18*). In sharp contrast, although the ovaries were proposed to be an ideal physiological model to study angiogenesis (*19*, *20*), the majority of knowledge of ovarian angiogenesis was gained from the pioneering study focusing on the corpus luteum (CL) (*20*), a follicle-derived temporary endocrine structure. Meanwhile, the lack of systematic studies on the spatial and temporal model of ovarian angiogenesis and on the physiological significance of adult ovarian angiogenesis has made the proposal to control female fertility by manipulating angiogenesis difficult to realize.

With the advantages of tissue-transparent technologies, the visualization of three-dimensional (3D) structures inside tissues (*21*–*25*) has been achieved in the past decade, which has greatly improved our understanding of organ development. By staining the blood vessels in transparent ovaries with an exogenous fluorescent label, the 3D localization and general changes of the ovarian vascular network have also been described (*26*, *27*). This pioneering study uncovered the essential roles of the vasculature in organizing follicles in the ovaries, but the limited resolution made the detailed model of ovarian angiogenesis and the pattern of ovarian vascular remodeling difficult to determine. By combining an endogenous genetic approach, especially multifluorescent reporter mouse models, with high-resolution imaging technology, our previous study traced the ovarian cell lineage and identified ovarian cell structures at the single-cell level in vivo (*28*, *29*). These mouse models and study systems provided ideal tools for imaging the detailed pattern of ovarian angiogenesis in vivo and guaranteed both the specificity and high resolution of labeled cells in the tissue.

In the current study, we combined transparent technologies with endogenous multicolor reporter mouse models and created a single-cell resolution, tissue-scale 3D imaging system for the detailed imaging and tracing of the angiogenesis process and vascular remodeling in whole ovaries and live ovarian follicles. On the basis of the characteristics of ovarian angiogenesis observed in our imaging and tracing results, we tested the long-term fertility effect of blocking adult angiogenesis in living mammals through the administration of Axi. Our further mechanistic study revealed that appropriate long-term suppression of adult angiogenesis reduced ovarian follicle consumption and postponed ovarian aging, which led to an extension of the female reproductive life span in aged females. In summary, the current study uncovered the detailed model of adult angiogenesis and vascular remodeling in mammalian ovaries and supplied

[1]State Key Laboratory of Agrobiotechnology, College of Biological Sciences, China Agricultural University, Beijing 100193, China. [2]Department of Cellular and Genetic Medicine, School of Basic Medical Sciences, Fudan University, Shanghai 200032, China. [3]Department of Microbiology, Tumor and Cell Biology, Karolinska Institute, Stockholm 171 77, Sweden.
*Corresponding author. Email: huazhang@cau.edu.cn

experimental evidence showing that the suppression of adult angiogenesis was an efficient target to postpone female reproductive aging, implying a potential clinical approach to retain the capability of female reproduction.

RESULTS

High-resolution 3D imaging of adult ovarian angiogenesis in mice

To investigate the profile of angiogenesis dynamics in the ovaries, we built a whole-mount imaging system to visualize ovarian blood vessels with a single-cell resolution. This was achieved by combining a vascular endothelium–specific endogenous dual-fluorescent tracing mouse model [tyrosine kinase (*Tek*)–*Cre;mTmG* mice] (*30*, *31*) with a modified 3D tissue-transparency technique (Fig. 1A) (*24*), followed by scanning the transparent tissues under a high-resolution spinning-disc confocal microscope (Fig. 1B). As shown in Fig. 1C, the whole-mount imaging system allowed us to image the 3D ovarian blood vessel network, including the capillaries, with high resolution on the scale of a whole mount (Fig. 1C and movie S1) and to analyze the subcellular structures (Fig. 1C, arrows) of a single blood vessel endothelium in detail.

With this system, we reconstructed a 3D model of *Tek-Cre;mTmG* ovaries at different reproductive stages to investigate the developmental changes of ovarian blood vessels. With ovarian development, the whole-mount images showed that a marked accumulation of blood vessels (Fig. 1D) occurred in ovaries from puberty onset [postnatal day (PD) 23] to adulthood (PD35 and 4 months). Quantification of the density of ovarian blood vessels confirmed a significant increase in blood vessels in the ovaries with the activity of female reproduction (Fig. 1E), showing a continuous activity of angiogenesis in the adult ovaries. In addition, our 3D imaging results showed a significant decrease in the blood vessel density in the ovarian stroma in 14-month-old females compared with that in 4-month-old females (fig. S1, A to C), indicating that a degeneration of ovarian blood vessels was accompanied by ovarian aging.

The spatial analysis of the image showed that blood vessels mainly existed in the stromal region of the ovaries (fig. S2A, arrows) and on the theca area surrounding the ovarian follicles (fig. S2B, arrows, and movie S2), but they were not observed inside the follicles (fig. S2B, arrowheads) or in the ovarian surface epithelium (fig. S2A, arrowheads). This is consistent with previous observations of avascular granulosa cells (GCs) in the follicles of ovaries (*32*). We also found that the density of blood vessels in the medulla stroma area was significantly higher than that in the ovarian cortical area (fig. S2, C to E) and that the average diameter of blood vessels in the medulla region was significantly wider than that in the cortical stroma region (fig. S2, C, D, and F). These results suggest that the stable blood vessels mainly localize in the medulla region of the ovaries. Moreover, our whole-mount imaging also revealed a dynamic development of blood vessels in the ovaries during the estrous cycle and demonstrated that the density of ovarian blood vessels in the ovaries during the proestrus period was significantly higher than that in the estrus, metestrus, and diestrus stages (fig. S3, A and B), indicating that angiogenesis was active with the fast growth of follicles.

Analyzing the localization and development of tip cells revealed an angiogenesis model in adult ovaries

We next analyzed the details of angiogenesis in the ovarian images to investigate the pattern of vascular remodeling in adult ovaries.

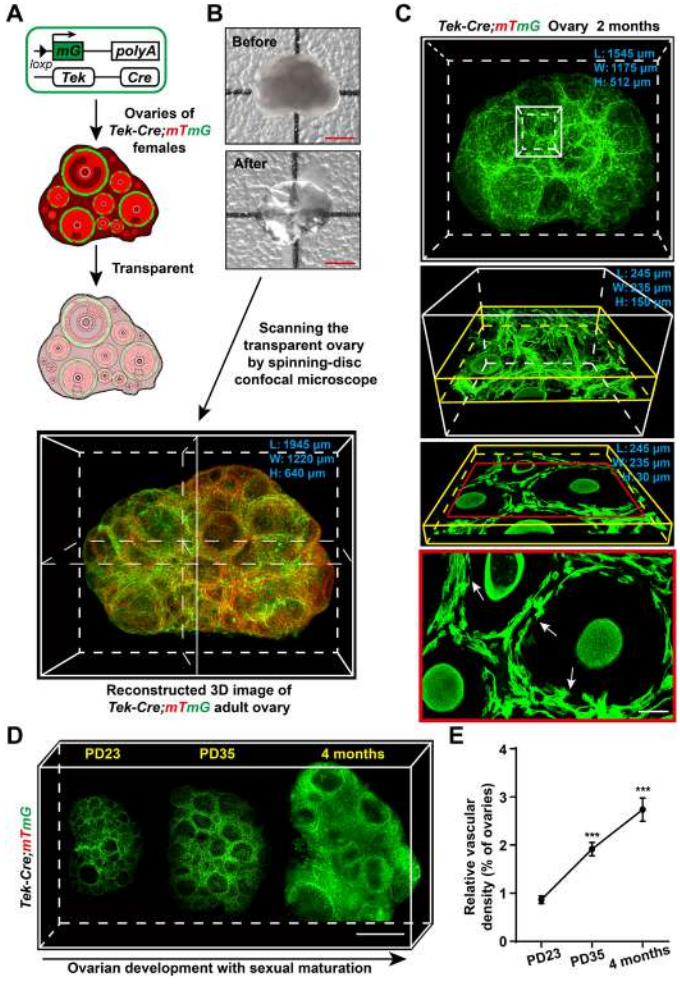

Fig. 1. High-resolution 3D imaging to reconstruct adult ovarian blood vessels in mice. (**A** and **B**) Schematic diagram showing the strategy used to achieve high-resolution 3D imaging of ovarian blood vessels. In *Tek*-expressing endothelial cells, Cre recombinase mediated a switch from mTomato (red) to mGFP (green). The *Tek-Cre;mTmG* ovaries with the mG-labeled endothelium were fixed and cleared (A), and the transparent ovaries were scanned by high-resolution confocal microscopy to reconstruct a 3D image of the ovarian blood vessels (B). (**C**) The reconstructed 3D images of *Tek-Cre;mTmG* ovaries were kept at a high resolution and were available for different analysis scales from the whole-organ level (white box) and single-follicle level (yellow box) to the subcellular resolution (red frame). The subcellular structures (arrows) are shown in the image. (**D**) Reconstructed ovarian blood vessels at the organ level showing a significant accumulation of blood vessels in mouse ovaries with sexual maturation, from puberty onset at PD23 to adulthood at 4 months. (**E**) Quantification of the relative changes in ovarian vessel density showing a significant increase in ovarian vessel density from PD23 to 4 months ($n = 9$ ovaries per group). The data are presented as means ± SD. The data were analyzed by a two-tailed unpaired Student's *t* test and ***$P < 0.001$. Scale bars, 500 μm (B and D) and 25 μm (C).

Through the scanning of the 3D-reconstructed ovarian vascular network at single-cell resolution, tip cells, which are the marker cells of angiogenesis (*33*–*36*), were clearly identified by their typical filopodia (Fig. 2, A and B, arrows) on green fluorescent protein (GFP)–labeled blood vessels. In the adult ovaries, we found that tip cells were abundantly distributed on the capillaries of growing follicles (GFs) [Fig. 2, A and C; $(8.9 \pm 4.1) \times 10^3/mm^3$] and in the CL [Fig. 2C and

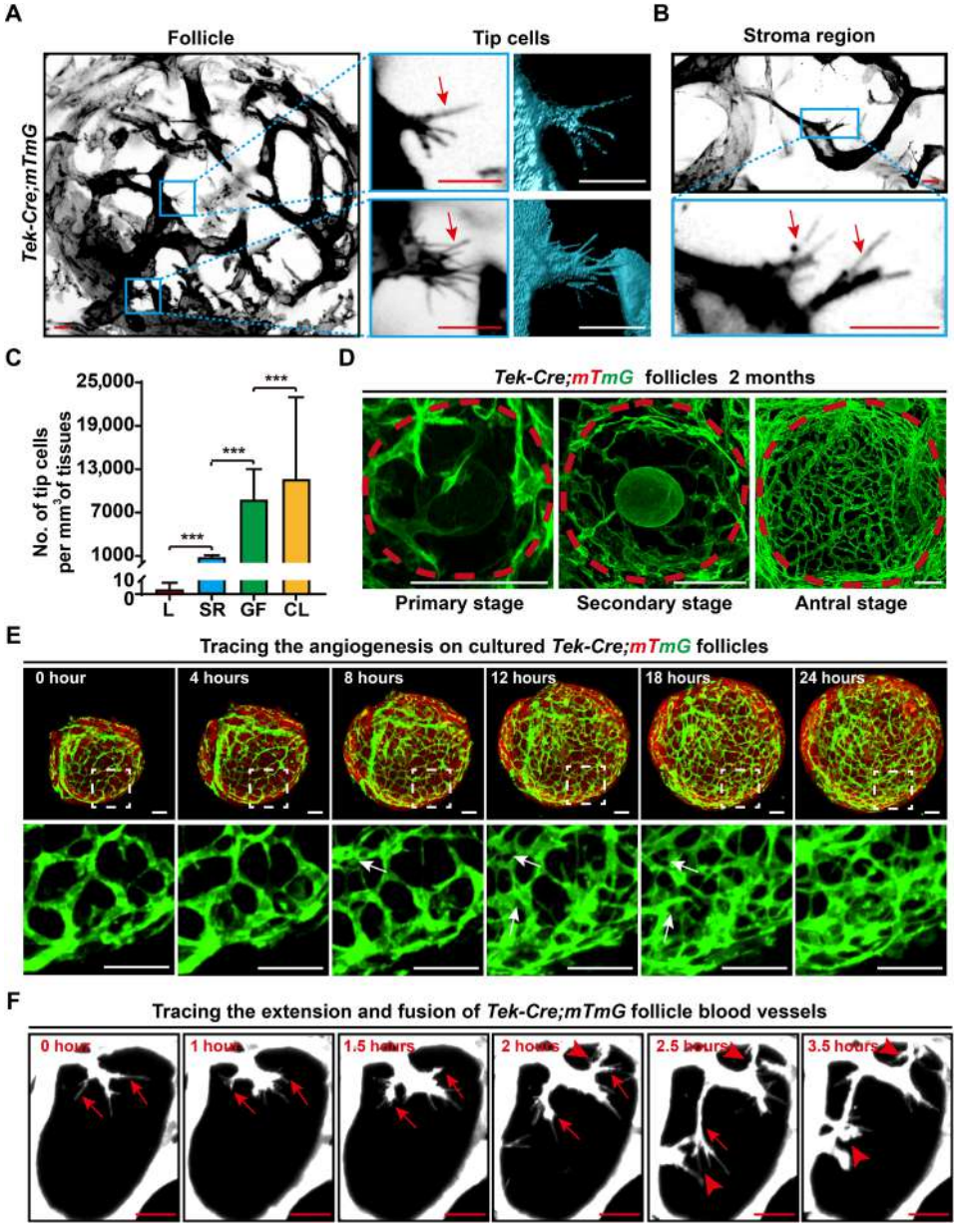

Fig. 2. Imaging and tracing angiogenesis in adult ovaries. (**A** and **B**) Analysis of the 3D-reconstructed ovarian images at the single-cell level to reveal the pattern of angiogenesis in the adult ovaries. Tip cells with filopodia (arrows) were mainly observed on the endothelium of GFs (A), and a few tip cells were randomly detected in the ovarian stromal region (B). (**C**) Quantification of the tip cell number in the liver (L), stromal region (SR), growing follicles (GFs), and CL of ovaries ($n = 20$ for each group) in adult mice (2 months), showing the abundance of tip cells in the adult ovaries, especially on GFs and CL. (**D**) Reconstructed images of ovarian follicles at different stages, showing a significantly increased density of blood vessels from primary follicles to antral follicles. (**E**) Live-cell imaging analysis recorded a marked growth of blood vessels on the surface of *Tek-Cre;mTmG* follicles. During 24 hours of in vitro culture, branching and extension were observed on the membrane GFP–labeled follicle endothelium (see movie S3). (**F**) High-magnification time-lapse imaging showing the behaviors of tip cells on follicle blood vessels (white). The extension of filopodia (arrows) on tip cells and the fusion of different tip cells (arrowheads) were recorded (see movie S4). GFP was converted to black and white in (A) and (B) to highlight the cell details. The data are presented as means ± SD. The data were analyzed by a two-tailed unpaired Student's *t* test and ***$P < 0.001$. Scale bars, 10 μm (A and B), 50 μm (D and E), and 25 μm (F).

fig. S2A, arrows; $(1.2 \pm 1.1) \times 10^4/mm^3$]. In sharp contrast, only a few tip cells were observed in the stromal region of the ovaries [Fig. 2, B and C; $(8.0 \pm 3.0) \times 10^2/mm^3$], and few tip cells were detected on blood vessels in the control adult liver (Fig. 2C and fig. S2B; $3.2 \pm 4.9/mm^3$). These results showed that adult angiogenesis was mainly active on GFs and their derived structure (CL) in the ovaries. Furthermore, our 3D images showed that the follicular capillaries presented a reticular structure surrounding the follicles and that the density of follicular capillaries was significantly increased with the maturation of follicles (Fig. 2D and fig. S3A), confirming continuous angiogenesis on ovarian follicles.

To further investigate how the follicle vascular network is constructed through angiogenesis in detail, we cultured isolated follicles at the secondary stage from *Tek-Cre;mTmG* females with a modified

3D living follicle in vitro development system (*37*) to observe the live process of angiogenesis and follicle vascular network construction. During 24 hours of in vitro culture, we found a marked branching and extension of mGFP (mG)–labeled blood vessels with follicle development that formed a high-density capillary bed on the follicle surface (Fig. 2E and movie S3). In detail, the fast increase in the follicle blood vessels presented an intussusceptive model (Fig. 2E, arrows) to increase the density of the vascular network. Meanwhile, the cell behavior analysis also showed that a clear tip cell–related extension of blood vessels on follicles (Fig. 2F, arrows) to increase the number of new vessel branches and clear fusions of the extended vascular endothelial cells (Fig. 2F, arrowheads) on these newly formed vessel branches constructed new blood vessels (Fig. 2F and movie S4). These results demonstrated that the active angiogenesis of follicles followed a complicated angiogenesis model to construct the follicle vascular network. Therefore, our imaging results showed that active adult angiogenesis constructs and remodels follicle blood vessels with ovarian development and that ovarian follicles are the active center of unique adult angiogenesis in the ovaries under physiological conditions.

Angiogenesis established independent and temporary vascular network for each follicle in adult ovaries

The imaging results revealed that ovarian follicles were the active center for the construction of the ovarian vascular network through angiogenesis. However, ovarian follicles are temporary structures with cyclic recruitment and regression (*1*) during adult life. Therefore, we next extended our study to investigate the fate of angiogenesis-formed new blood vessels on the follicles in the ovaries. To trace the development of the follicle vascular endothelium in vivo, we introduced a multicolor fluorescent reporter *Tek-Cre;Rainbow* mouse model (*38*), in which *Tek*-positive vascular endothelial cells randomly expressed red (RFP), orange (OFP), or cyan (CFP) fluorescent proteins (fig. S4A), allowing them to be distinguished from *Tek*-negative GFP-expressing cells (fig. S4B). With this model, we seeded *Tek-Cre;Rainbow* GFs into the ovaries of wild-type recipient females through surgery and traced the developmental fates of these fluorescent follicles in vivo (Fig. 3A). Before transplantation, all isolated *Tek-Cre;Rainbow* follicles were surrounded by fluorescent blood vessels (Fig. 3B, arrows), showing a comprehensive follicle structure for subsequent in vivo tracing. After 2 weeks of seeding, the transplanted follicles presented a sufficient survival rate in the recipient ovaries (ROs) (87.8%, 86 of 98 checked ROs with transplanted fluorescent follicles) and developed to further stages, including antral follicles (Fig. 3C, arrows) and CL (Fig. 3C, arrowheads). Moreover, ovulated GFP oocytes (Fig. 3D, arrows) were obtained from recipient females, demonstrating the normal development of transplanted follicles in ROs, and our tracing system successfully mimicked physiological follicle development in vivo.

With a focus of fluorescent blood vessels on transplanted follicles, we observed fluorescent blood vessels on all of the detected fluorescent follicles, and they developed with follicle growth. This result demonstrated a successful connection of the donor vascular system with the recipients. Furthermore, a high-density vascular network with different colors of fluorescence was clearly observed in the transplanted follicle–derived CL (Fig. 3E, CL), revealing normal angiogenesis of transplanted follicle blood vessels. We found that no fluorescent blood vessels extended to the ROs to cover the recipient follicles, even those closely adjacent to the transplanted follicles (Fig. 3E, arrows). This result indicated that although robust angiogenesis was active on the follicles, the extension of blood vessels through active follicular angiogenesis was limited in the follicle theca layer; therefore, each follicle formed an independent vascular network to support its development. At 2 months after transplantation, almost all transplanted ovaries contained no fluorescent follicles (97 of 98), indicating the exhaustion of transplanted follicles in the recipient females (fig. S4C). Consistent with the exhaustion of transplanted follicles, no fluorescent blood vessels were found in the ROs (Fig. 3F and fig. S4C), demonstrating the complete elimination of follicle-related blood vessels in the ovaries. Therefore, we conclude that active angiogenesis forms a complex but independent blood vessel network for each follicle and that these newly formed blood vessels are completely eliminated with follicle atresia or ovulation (Fig. 3G).

Axi treatment disrupted follicle blood vessel construction but kept the ovarian reserve in adult females

Our findings revealed that adult angiogenesis was mainly active on follicles to construct temporary and independent vascular networks in ovaries. This pattern implied that the proper suppression of adult angiogenesis should mainly affect the existing GFs, which were blood vessel dependent, but might have no severe effects on the ovarian reserve, which had no individual blood vessels (*39*–*41*).

To support our hypothesis, we next designed experiments to block adult angiogenesis in living animals. The angiogenesis inhibitor Axi was intraperitoneally injected [30 mg/kg body weight (BW), every other day] into the *Tek-Cre;mTmG* females to suppress the activity of angiogenesis in vivo for 1 month beginning at 2 months of age (Fig. 4A), and an identical increase in BW in the Axi and control groups showed no marked side effects (fig. S5A) during the drug-treated period. After the treatment, we first checked the effects of blood vessel development in the ovaries and other organs by performing high-resolution transparent imaging. As expected, a marked decreased density of mG-labeled blood vessels was found on the ovarian follicles in Axi-treated mice compared with those of control mice (Fig. 4, B and C). In sharp contrast, there were no marked changes in blood vessel density in the ovarian stromal region (Fig. 4, B and C) or liver (Fig. 4, B and C) between the Axi and control groups. These results indicated that our Axi treatment strategy mainly suppressed angiogenesis by blocking the establishment of a new follicle vascular network but had little effect on stable blood vessels.

To determine the effect on folliculogenesis, histological analysis was performed, showing that the size of ovaries was notably decreased, and no preovulatory follicles or CL (Fig. 4D) existed in the treated ovaries. Follicle count results confirmed a decreased number of GFs in the Axi-treated ovaries compared with the controls (Fig. 4E; 193 ± 35 versus 354 ± 35). Unexpectedly, the decreased number of GFs did not lead to a diminished ovarian reserve in Axi-treated ovaries. On the contrary, the total number of follicles in the Axi-treated ovaries was much greater than that in the control ovaries (Fig. 4F; 1440 ± 189 versus 1120 ± 123) because of a significantly increased number of primordial follicles (PFs) (Fig. 4, G and H; 1247 ± 182 versus 766 ± 99) in the cortical region of ovaries after Axi treatment (Fig. 4G, arrows, and fig. S5B, arrows). Since dormant PFs represent the ovarian reserve and cannot be renewed in adult ovaries (*29*), our results indicate that the suppression of adult angiogenesis reduces the loss of PFs and keeps the ovarian reserve in females.

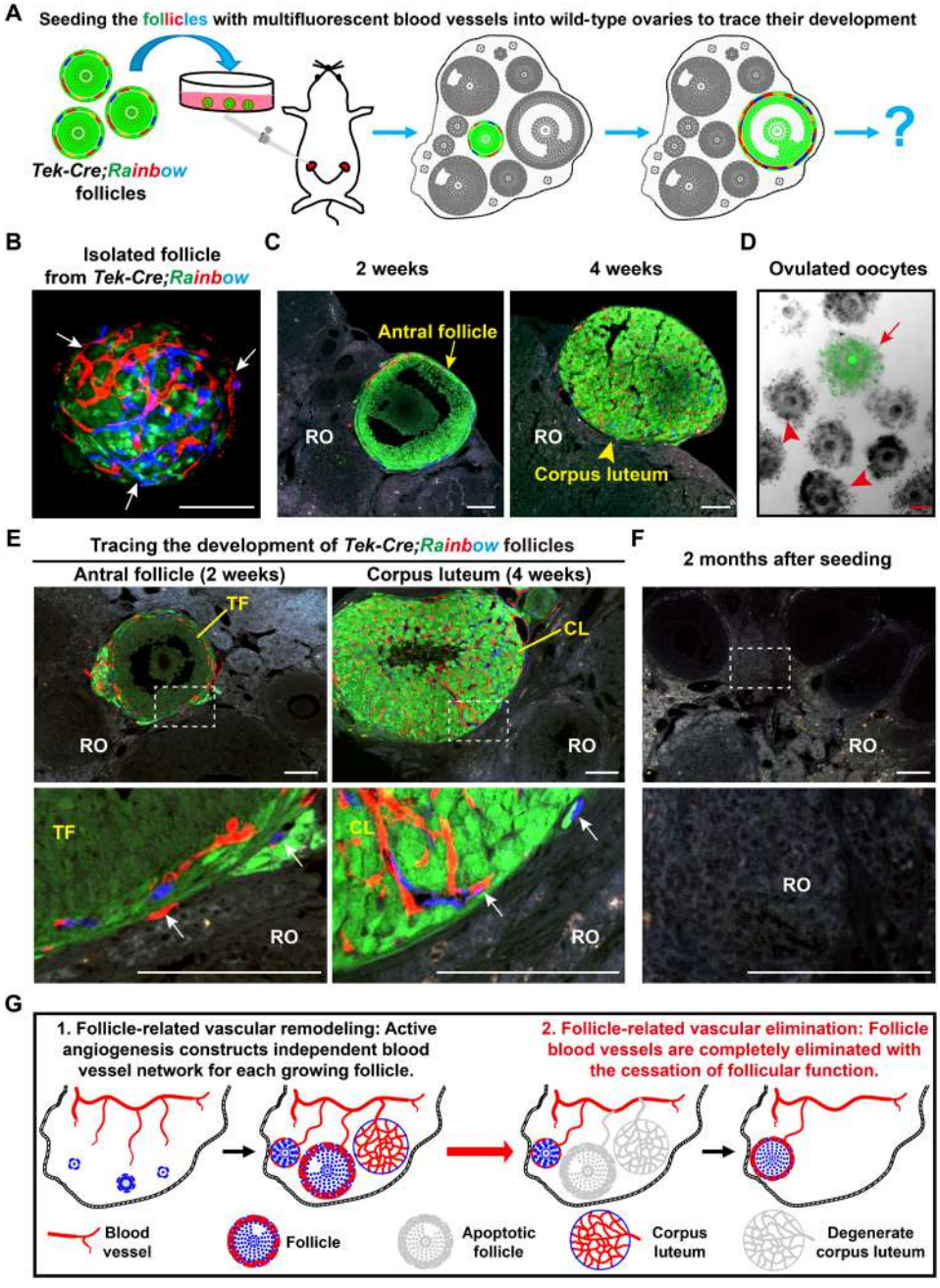

Fig. 3. Angiogenesis established an independent and temporary follicle vascular network in the adult ovaries. (**A**) Illustration of the strategy used to trace the development of follicle blood vessel endothelial cells in vivo. GFs with fluorescent-labeled blood vessels were isolated from *Tek-Cre;Rainbow* females and were surgically seeded into the ovaries of wild-type recipient females for long-term tracing. (**B**) Before seeding, a single follicle from *Tek-Cre;Rainbow* ovaries showed red or blue fluorescent blood vessels (arrows) surrounding the GFP follicle. (**C** and **D**) The transplanted *Tek-Cre;Rainbow* follicles successfully developed to the antral stage and formed a CL in the recipient ovaries (ROs) and also ovulated the GFP oocytes from recipient females, showing the normal development of the seeded follicles. (**E**) Tracing the developmental fate of follicle blood vessels after transplantation. All fluorescent blood vessels (arrows) were limited to the surface of transplanted follicles and the CL, which were derived from transplanted follicles. (**F**) At 2 months after seeding, all fluorescent blood vessels were eliminated because of the exhaustion of transplanted follicles in the ROs (0 of 97). The transplanted window is indicated by the white frame. (**G**) Schematic of the fate of new follicular blood vessels formed via angiogenesis, showing the formation of an independent blood vessel network for each GF in the ovaries, and a complete elimination of follicle blood vessels with the cessation of follicle function. RO, recipient ovary; TF, transplanted follicle; CL, corpus luteum. Scale bars, 100 μm (B to E).

Blocking angiogenesis paused ovarian development in females

We next investigated the underlying mechanisms of how blocking angiogenesis protects the ovarian reserve in females. The rate of follicle loss in ovaries is mainly determined by the balance of GF recruitment and PF dormancy (*1*, *42*). Since the blocking of angiogenesis mainly suppressed the construction of a vascular network on the GFs, we proposed that angiogenesis-related blockage of blood

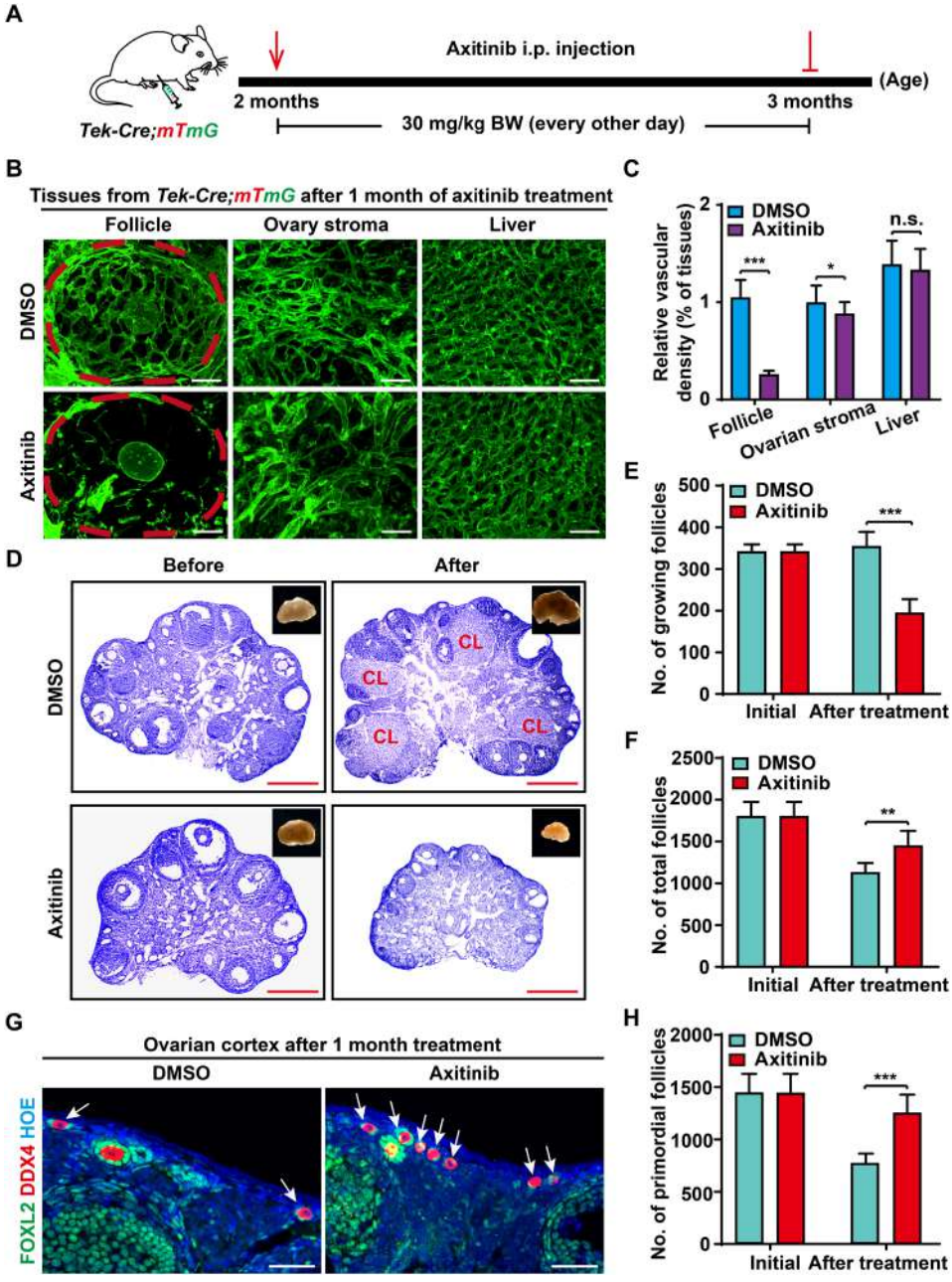

Fig. 4. Axi treatment disrupted follicle blood vessel construction but kept the ovarian reserve in adult females. (**A**) The strategy of Axi treatment in females. Females at 2 months were treated with Axi (30 mg/kg BW, every other day) for 1 month to temporarily block angiogenesis. i.p., intraperitoneal. (**B**) After 1 month of Axi treatment, a significantly decreased vascular density was observed on the follicles of Axi-treated ovaries compared with those in the DMSO group ($n = 8$), but no marked effect was found for the stable blood vessels of the ovarian stromal region and liver. (**C**) Quantification of vascular density in the follicles and stromal region of ovaries and the liver after Axi treatment ($n = 9$ ovaries per group). (**D**) Histological analysis showed the decrease in ovarian size and in the number of GFs in the Axi group compared with the controls. (**E**) Follicle counts showed a significant decrease in the number of GFs in the Axi-treated ovaries ($n = 6$). (**F**) The total follicle number in the Axi-treated and control ovaries, showing that the total number of follicles in the Axi group was significantly greater than that in the controls ($n = 6$). (**G**) Immunostaining results revealed more primordial follicles (arrows) in the cortex of Axi-treated ovaries. Green: anti-FOXL2/GCs. Red: anti-DDX4/oocytes. Blue: Hoechst33342. (**H**) Follicle count results of primordial follicles (PFs), showing an increased number of PFs in Axi-treated ovaries compared with the controls ($n = 6$). The data are presented as means ± SD. The data were analyzed by a two-tailed unpaired Student's *t* test; $^{***}P < 0.001$, $^{**}P < 0.01$, $^{*}P < 0.05$, n.s. $P \geq 0.05$. Scale bars, 50 μm (B and G) and 500 μm (D).

vessel construction might directly affect the development dynamics of GFs.

To measure the development dynamics of GFs in vivo, we created Zona pellucida protein 3 (*Zp3*)-*CreER*^{T2} mice (fig. S6A) and crossed them with *mTmG* reporter mice to establish an inducible follicle growth–tracing mouse model (*Zp3-CreER*^{T2}*;mTmG* mouse model). In this model, *Zp3*-positive oocytes in GFs could be inducible labeled by GFP (mG) through tamoxifen (Tam) administration, which

allowed us to label the growing oocytes and to trace the life span of existing GFs in vivo (Fig. 5A). Validation of the *Zp3-CreER^{T2};mTmG* model demonstrated sufficient labeling efficiency and specificity to trace the developmental dynamics of the GFs (Fig. 5B), and approximately half of GFs (Fig. 5B, arrows; 56.4 ± 2.1%) and no dormant PFs (Fig. 5B, arrowheads) were labeled after 7 days of Tam treatment. The *Zp3-CreER^{T2};mTmG* females after 7 days of Tam treatment from 2 months old are referred to as "GF-labeled" females (Fig. 5C) here.

We next treated GF-labeled females with or without Axi (30 mg/kg BW, every other day) for 1 month and measured the developmental

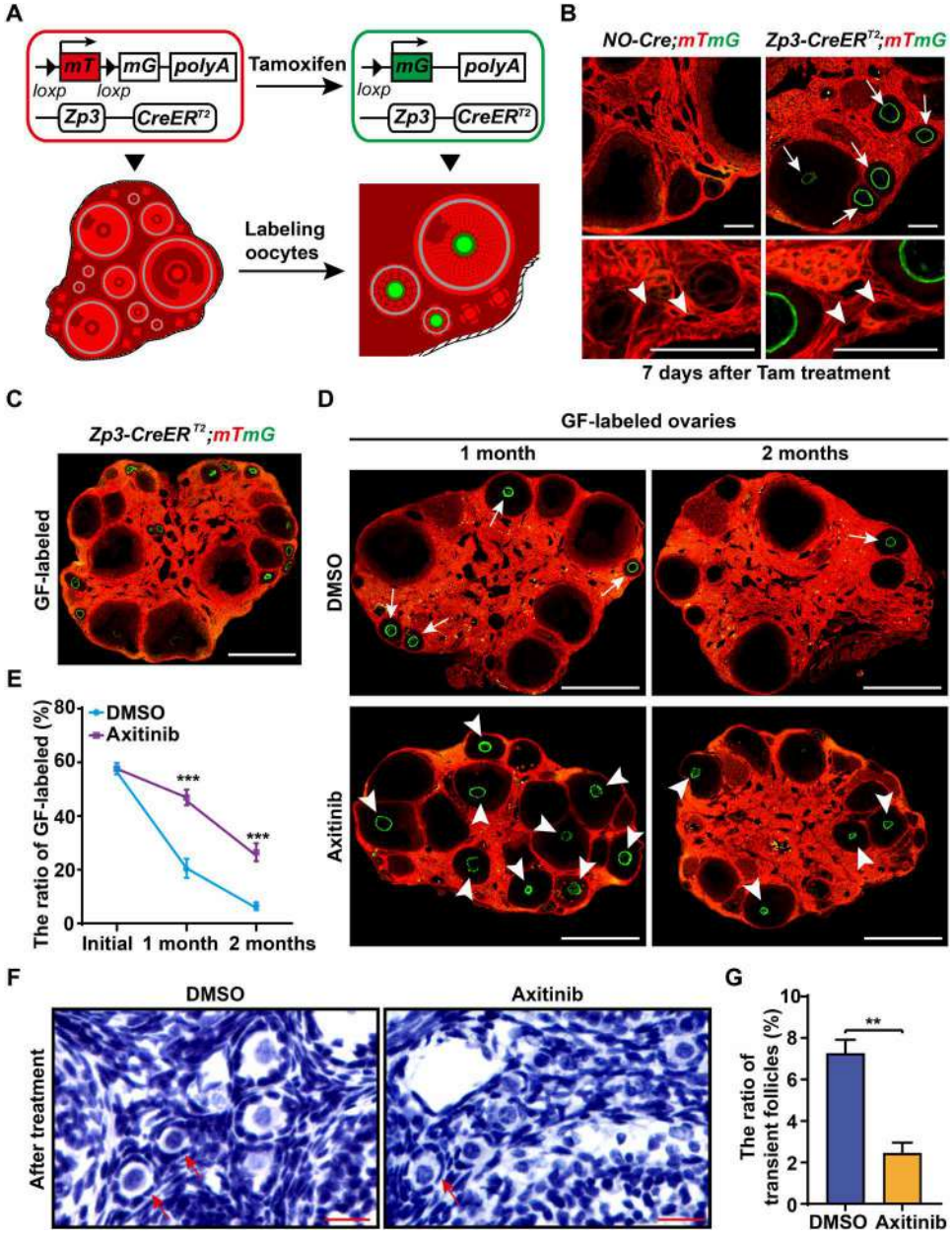

Fig. 5. Blocking angiogenesis paused ovarian development. (**A** and **B**) Illustration of tamoxifen (Tam)–induced labeling of growing oocytes in the *Zp3-CreER^{T2};mTmG* mice. CreER^{T2} recombinase is active upon Tam induction, which mediates the switch from mTomato (red) to mGFP (green) in Zona pellucida protein 3 (*Zp3*)–expressing oocytes, resulting in the labeling of GFs with green oocytes. (**B**) Validating the labeling specificity and efficiency of *Zp3-CreER^{T2};mTmG* females. After 7 days of Tam treatment, numerous oocytes in GFs were labeled with mG (arrows), whereas none of the dormant oocytes (arrowheads) were labeled in the *Zp3-CreER^{T2};mTmG* ovaries. (**C**) The 2-month *Zp3-CreER^{T2};mTmG* females after 7 days of Tam treatment are referred to as "GF-labeled" females. (**D**) Tracing the developmental dynamics of GFs in GF-labeled females with or without Axi treatment. GFP oocytes (arrowheads) were widely distributed in GF-labeled ovaries at either 1 or 2 months in Axi-treated females but were exhausted in control ovaries after 2 months (arrows). (**E**) Quantification of the labeling ratio of the GF showed a significant extension of GF life span in Axi-treated ovaries ($n \geq 6$). (**F**) Histological identification of the transient follicles (arrows) in the controls and Axi-treated ovaries. (**G**) Counting the transient follicles showed a significantly decreased ratio of transient follicles in the Axi-treated ovaries compared with the controls ($n = 5$). The data are presented as means ± SD. The data were analyzed by a two-tailed unpaired Student's *t* test; ***$P < 0.001$, **$P < 0.01$. Scale bars, 100 μm (B), 500 μm (C and D), and 25 μm (F).

profile of labeled follicles at different time points. In the control ovaries, a marked decreased number of labeled follicles was observed in the ovaries after 1 month (Fig. 5D), and few labeled follicles (Fig. 5D, arrows) were found at 2 months after labeling, showing an exhaustion of recruited GFs during 2 months of development. In sharp contrast, GFP-labeled oocytes were widely distributed in the Axi-treated ovaries after either 1 or 2 months of treatment (Fig. 5D, arrowheads). The quantification of the ratio of labeled follicles confirmed that approximately 25.3 ± 3.3% of growing oocytes with GFP labeling existed in the 2-month Axi group (Fig. 5, D and E), whereas only 5.8 ± 1.4% of labeled follicles existed in the control ovaries. These results showed that the life span of GFs was notably extended when angiogenesis was suppressed.

The other key index of ovarian reserve consumption, the ratio of PF activation (*42*), was also investigated by counting the transient follicles that were identified by mixed flattened (fig. S6B, arrows) and cuboidal (fig. S6B, arrowheads) GCs of follicles in the ovaries. Although the transient follicles were observed in both Axi-treated ovaries and controls (Fig. 5F, arrows), a significantly decreased ratio of transient follicles in total PFs was found in Axi-treated ovaries compared with that in controls (Fig. 5, F and G), showing that angiogenesis blockage decreased the activation of PFs in ovaries. Combined with the phenotype revealed by GF tracing, our results showed that the appropriate suppression of adult angiogenesis directly increase the life span of existing GFs and indirectly decrease the recruitment of dormant PFs, thereby pausing ovarian development and preserving the ovarian reserve in adult life.

Appropriate inhibition of adult angiogenesis extended the reproductive life span of aged females

Our results suggested that appropriately blocking adult angiogenesis is beneficial for female reproduction. We next tested whether Axi-mediated angiogenesis blockage could affect the female fertility in the long term. We chose females at midreproductive age (7 months old) and treated them with Axi (30 mg/kg BW, every other day) for 1 month (Fig. 6A), and an identical increase in BW (fig. S7A) in the Axi and control groups during the drug-treated period confirmed no marked side effects in the females. After 1 month of Axi treatment, the follicle counts confirmed a protective effect of Axi treatment on the ovarian reserve [fig. S7, B (arrows) and C] in 8-month-old females. We found that this protective effect of the ovarian reserve was sustained in the females to 14 months, and more PFs and total follicles were present in treated ovaries compared with the controls (Fig. 6, B and C) in aged females. Histological analysis also showed that the Axi-treated ovaries exhibited a clearly younger status with more follicles and CL (Fig. 6B, arrows), which was in sharp contrast to the atrophy of the control ovaries.

Next, we investigated the reproductive capability of females after angiogenesis blocking. After 1 month of Axi treatment, the females (7 months old) were mated with healthy fertile males to evaluate their fertility. At the first 4 months of mating, a comparable number of offspring were born from Axi-treated and control females, showing no negative effect of the termination of Axi treatment on female fertility (fig. S7D). With aging, all control females ceased producing offspring at the age of 12 months (Fig. 6D), as expected (*43*, *44*). In sharp contrast, most females after Axi treatment continued to produce offspring until 14 months of age (Fig. 6D), showing a significantly extended reproductive life span after treatment at an early age. Hormone detection showed significantly higher estrogen (E2) and progesterone (P4) levels and a lower follicle-stimulating hormone (FSH) level in the Axi-treated females than those in the controls at 14 months (Fig. 6, E and F, and fig. S7E), suggesting a young endocrine status of treated females (Fig. 6G). Therefore, our results indicate that the appropriate inhibition of adult angiogenesis extended the female reproductive life span in mice, and blocking angiogenesis

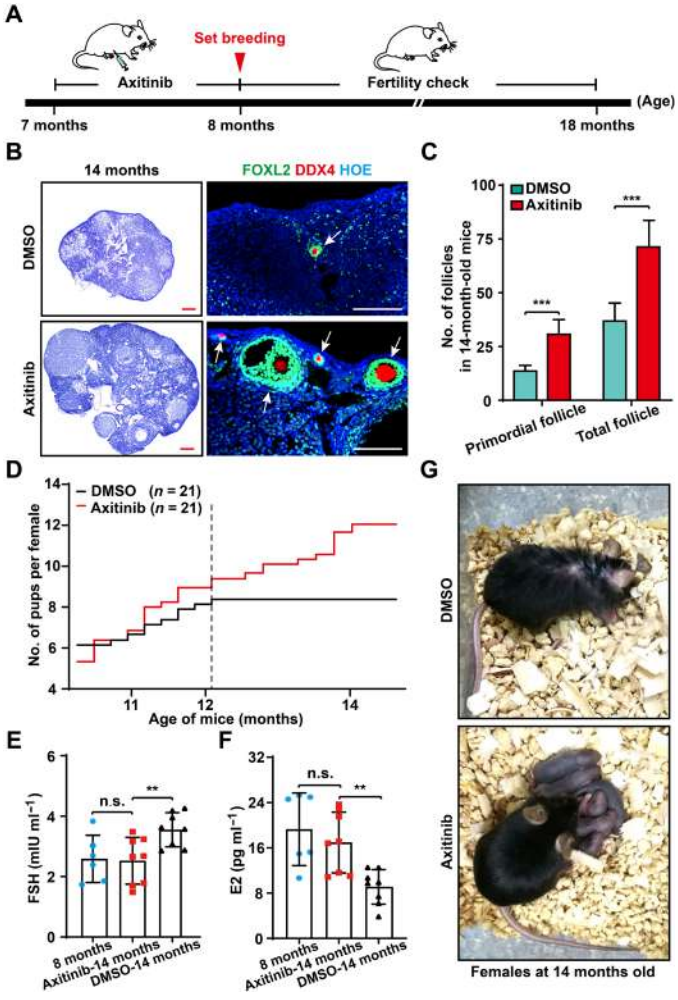

Fig. 6. Appropriate inhibition of adult angiogenesis extended the reproductive life span of aged females. (**A**) The strategy of Axi treatment in females of late reproductive life span. After 1 month of Axi or vehicle treatment, females at 8 months were mated to check their fertility and were used to detect other reproductive-related indices at different time points. (**B**) Histological analysis showing Axi-treated ovaries exhibited a clear younger status at 14 months with many follicles (arrows) compared with the control ovaries. (**C**) Follicle counting results showing that more follicles survived in the Axi-treated ovaries compared with the controls at the age of 14 months ($n = 6$). (**D**) Fertility test results showed a significant extension of the female reproductive life span after Axi treatment ($n = 21$). (**E** and **F**) The sex-related hormones, including follicle-stimulating hormone (FSH) and estrogen (E2), were found to be comparable in untreated females at 8 months and Axi-treated females at 14 months of age, whereas significantly increased levels of FSH and decreased levels of E2 were detected in the 14-month-old females of the DMSO group ($n = 8$ per group). (**G**) The general appearance of Axi-treated and the control females at 14 months, showing healthy pups with Axi-treated mothers (Photo credit: Xueqiang Xu, China Agricultural University). The data are presented as means ± SD. The data were analyzed by a two-tailed unpaired Student's *t* test; $^{***}P < 0.001$, $^{**}P < 0.01$, n.s. $P \geq 0.05$. Scale bars, 100 μm (B).

should be an efficient approach to improving female reproductive health in mammals.

DISCUSSION

This study provided comprehensive descriptions of the model of adult ovarian angiogenesis and the developmental pattern of ovarian blood vessels in mammals. Through a series of imaging and tracing experiments, we clarified not only that the GFs and their derived structure (CL) are the center of angiogenesis in adult ovaries but also that all follicle-related blood vessels are temporary circulatory structures that are eliminated completely after ovulation or atresia. Furthermore, we demonstrated that blocking the construction of angiogenesis-built new blood vessels is an efficient strategy to pause the development of ovaries in living animals, which ultimately postpones ovarian aging and extends the reproductive life span of females.

By identifying the proliferated vascular endothelium and analyzing the ultrastructure of the CL capillaries by electron microscopy, it was reported that the rapid growth of endothelial cells in the CL contributed to female reproduction (*32*, *45*). These pioneering findings revealed a unique regeneration of new blood vessels and active angiogenesis in the adult ovaries under physiological conditions. In the current study, we developed a modified organ transparent technology by combining reported enhanced-tissue clearing technology with a high-resolution large-scale imaging approach to detect 3D ovarian blood vessel profiles. Unique from previous reports, our whole-mount imaging system introduced an endogenous fluorescent endothelial labeling mouse model, in which blood endothelial cell outlines are visualized by membrane GFP. This endogenous labeling system allowed us to take highly precise images at the organ level while retaining the in situ details of subcellular structures at the single-cell level. With the system, the reconstructed 3D images successfully revealed the changing profiles of blood vessels with the activity of female fertility at scales from the whole organ (whole ovary) to a multicellular structure (single follicle) to the single cell (tip cells). We believe that this system also has broad application potential for studying detailed models of in situ adult angiogenesis in various conditions, such as tumorigenesis.

Using this system, we also revealed that adult ovarian angiogenesis followed the classic tip cell–mediated model at the single-cell level, which is similar to pathological angiogenesis in the progression of tumorigenesis (*46*, *47*). By determining the positions of tip cells in our reconstructed ovarian blood vessels, we confirmed previous findings that the active generation of blood vessels occurs in the CL (*20*, *48*) and further clarified that GFs are the center of adult ovarian angiogenesis. It was an expected result that the remodeling and regeneration of blood vessels mainly occur on ovarian follicles since the orderly development of follicles is the major power driving the estrus cycle in females (*1*). In our tracing study, we found that each follicle formed an independent blood vessel system in the ovaries and that all follicle-related vascular networks were completely eliminated with the cessation of follicular function. Although it is known that CL blood vessels regress with ovarian development, it is unexpected that no recycling of follicle blood vessels occurs since the recruitment of follicles is sustained for approximately 50 years in humans. We believe that forming an independent and temporary blood vessel network may be a flexible strategy to guarantee the quality control of dominant follicles.

In modern society, the average life span has been markedly extended, but menopause occurs consistently at the approximate age of 50 in women (*49*, *50*). This contradiction has led to a great gap between aging and reproductive aging in females, which reduces later-life quality for all women (*51*, *52*). Although it is well known that the loss of ovarian follicles leads to female reproductive aging, there is no suitable strategy available to disrupt ovarian aging by manipulating follicle development. As the connector of the ovaries and the body, the blood vessels surrounding the follicle act as the primary regulator of ovarian development. Therefore, the possibility of manipulating angiogenesis to control female reproduction was proposed decades ago (*40*, *53*). The pattern of adult ovarian angiogenesis and the transience and independence of the follicle vascular network strongly imply that blood vessel remodeling in adult ovaries maintains fertility rather than the survival of ovarian tissue. This pattern further improves the feasibility of manipulating ovarian angiogenesis to protect against ovarian aging. By using a well-characterized small-molecule VEGFR inhibitor, Axi, we found that blocking adult angiogenesis should be an efficient way to reduce the loss of the ovarian reserve and suppress ovarian aging in females. We found that treatment with Axi at the early reproductive stage was able to extend the female reproductive life span in late life. Moreover, the use of Axi not only postpones female reproductive aging but also maintains a young hormone status for females, implying a general antiaging effect of this strategy. However, as a nonspecific inhibitor for angiogenesis, Axi might not be the ideal inhibitor for use in antifemale reproductive aging. Much more work should be performed to investigate the efficient drug or approach needed to specifically block angiogenesis in ovaries, and any relevant clinical practice should be treated with caution before finding a safe and effective approach.

Although much research remains to be done before this treatment can be applied in clinical practice, the current study supplied foundational information on angiogenesis patterns in adult ovaries. Furthermore, we provided direct evidence showing that suppressing adult angiogenesis is a highly feasible antiovarian aging strategy to extend female fertility and perhaps also the vitality of aged females. With the further understanding of ovarian angiogenesis, especially the discovery of ovarian-specific regulatory mechanisms of angiogenesis and ovarian-targeting drug delivery approaches, we believe that the application of an antiangiogenesis treatment to postpone reproductive aging will become a reality in the future.

MATERIALS AND METHODS

Experimental mice

C57BL/6 and ICR mice were from the Laboratory Animal Center of the Institute of Genetics (Beijing, China). The *Tek-Cre* mice [the Jackson Laboratory stock number 004128, B6.Cg-Tg (*Tek-Cre*)12 Flv/J] (*54*) were a gift from H. Chen. These transgenic mice express Cre recombinase under the direction of the receptor Tek promoter, which has been shown to provide uniform expression in endothelial cells during embryogenesis and adulthood. The transgene integrated into chromosome 13, causing a 241.3-kb deletion. The deletion results in a functional knockout of *Mtrr*, *Adcy2*, and *Fastkd3* in homozygous mice. Mice that are hemizygous for the transgenic insert are viable, fertile, normal in size, and do not display any gross physical or behavioral abnormalities. B6.Cg-Tg (*Tek-Cre*)12 Flv/J strain (*55*) germline deletion was prevented by restricting Cre expression to male

breeders. *Rainbow* and *mTmG* (007576, Jackson Laboratory) mice were generated as previously reported (*28*, *38*), and the *Rainbow* mice were a gift from K. Liu. *Tek-Cre* mice were crossed with *mTmG* and *Rainbow* mice to generate *Tek-Cre;mTmG* and *Tek-Cre;Rainbow* for genetic lineage tracing of Tek+ cells. In addition, to obtain *Tek-Cre* transgenic mice, we designed polymerase chain reaction (PCR) primers for Cre enzyme DNA sequence (forward: 5′-ATTTGCCTGCATTACCGGTC-3′, reverse: 5′-ATCAACGTTTTCTTTTCGG-3′).

The *Zp3-CreER^{T2}* transgenic mice were generated using CRISPR-Cas9–mediated genome engineering by the Nanjing BioMedical Research Institute of Nanjing University, the Model Animal Research Center of Nanjing University, Nanjing, China. Generally, the *Zp3-CreER^{T2}* knock-in mouse line was generated by inserting a cDNA-encoding Cre recombinase fused with a mutant form of the CreER^{T2} into frame with the translational start codon (ATG) of the *Zp3* gene, as previously described (*56*). The obtained mouse lines were crossed to C57BL/6 lines for germline transmission. We designed PCR primers spanning the genomic DNA and inserted cassette (forward: 5′-TGGTTCAGATGAGGTTTGAGGC-3′, reverse: 5′-CGCGAACATCTTCAGGTTCTGC-3′) to test the correct targeted allele. The established *Zp3-CreER^{T2}* mouse lines were maintained on a C57BL/6 background. Tam (75648, Sigma-Aldrich) was resuspended in 95% (v/v) ethanol (100 mg/ml) and then diluted in corn oil (C8267, Sigma-Aldrich) to a final concentration of 20 mg/ml. To label the growing oocytes in the ovaries of *Zp3-CreER^{T2};mTmG* females, Tam, at a dosage of 50 mg·kg^{-1} BW, was intraperitoneally injected for two continuous days in 2 months.

All mice were housed in mouse facilities under 16/8-hour light/dark cycles at 26°C with access to chow and water at libitum. The animal experiments conformed to the guidelines and regulatory standards of the Institutional Animal Care and Use Committee of China Agricultural University, no. AW52301202-3-1.

High-resolution 3D tissue imaging

The clearing method of the tissues is carried out according to the method described previously (*24*) with modifications. Generally, stock *N*-methylacetamide (M26305, Sigma-Aldrich) was prepared by diluting melted *N*-methylacetamide to 40% (v/v) in phosphate-buffered saline (PBS), which was then used to dissolve Histodenz (D2158, Sigma-Aldrich) to 86% (w/v) concentration. Then, Triton X-100 (0.1% v/v) and 1-thioglycerol (M1753, Sigma-Aldrich) (0.5% v/v) were added to the Histodenz solution to be the final clearing solution.

To image the ovarian vascular network, the ovaries at different ages were collected and washed with PBS containing 0.2% Triton X-100 and 1-thioglycerol (0.5%) in the dark for 24 hours at room temperature to remove blood cells. Then, the tissues were placed in the clearing medium (1:50 v/v) and incubated in the dark at room temperature on a rotor for 72 hours.

The cleared ovaries were embedded in a 35-mm dish with 14-mm glass bottom (D35-14-1-N, Cellvis) containing fresh clearing solution and tightly covered by a coverslip. Confocal imaging was performed on an inverted Leica (DMi8) and Andor Dragonfly spinning-disc confocal microscope, a scientific complementary metal-oxide semiconductor (sCMOS) camera (Andor Zyla 4.2), and using either a 20× 0.8 numerical aperture (NA) 650-μm working distance or a 40× 1.3 NA 250-μm working distance objective. A pixel density of 2048 × 2048 was used, and Z-step 0.5 to 1.0 μm for 650 μm (20× objective) or 0.3 to 0.6 μm for 250 μm (40× objective). The 488-nm (mG) and 568-nm mTomato (mT) lines of the Andor Integrated Laser Engine (ILE) system with a spinning-disc confocal scan head (Andor Dragonfly 500) were imaged. Images were acquired by Fusion 2.1 software (https://andor.oxinst.com/products/dragonfly#fusion).

After acquisition, movie S3 or single time point images were processed by ImageJ (http://rsbweb.nih.gov/ij/) for projection of all z stacks and merged color channels. To clearly highlight the filopodia structures of the tip cells, the mG (488 nm) channel was inverted to black and white by ImageJ software. To show the 3D vascular structure of ovaries and follicles and the fusion process of tip cells, the rotary 3D movie was processed by Imaris (https://imaris.oxinst.com/) software (movies S1, S2, and S4). To distinguish the follicle stages in the image, the size and the GC number were identified by mT in a single optical section (fig. S3A).

Quantification of the number of tip cells

To perform the quantitative analysis of tip cells in the reconstructed 3D ovarian imaging, the images were scanned carefully under the mode of 3D View and Slice in Imaris (https://imaris.oxinst.com/) software. In detail, the whole-mount imaging was separated to optical stacks (around 50 μm for stromal region and liver, or the whole follicle) in the *z* axis, and the identification of filopodia manually scanned the follicles or randomly selected optical stacks (for liver or ovarian stromal region) with focus of GFP-labeled blood vessels by a filament-tracing function in Imaris.

To count the tip cells on follicles or in CL, the total number of cells with filopodia on each follicle or CL was counted, and the mean number of tip cells was calculated by analyzing different follicles ($n = 56$) at same stages or CLs from more than six animals. To count the tip cells in the ovarian stromal region or liver, the number of tip cells was counted in randomly selected regions of ovaries without follicles (volume: 500 μm × 500 μm × 50 μm, 5 to 10 points per ovary), and the mean number of tip cells was calculated by analyzing the ovaries form three animals. The density of the tip cells in the tissues was counted by tip cell number to divide the tissue volume.

Follicle isolation and culture

The ovaries were dissected from *Tek-Cre;mTmG* mice at PD23, and the ovarian capsules were separated and removed in precooled PBS (10 mM, pH 7.4) under a stereomicroscope (Stemi 305, Zeiss) with sterile conditions. Follicles (average diameter: 318.9 ± 24.3 μm, $n = 45$) were separated by tearing ovaries with syringe needle.

To observe the detailed behaviors of angiogenesis on the follicles, the follicles were cultured on a Millicell culture insert (Millipore, Merck) with the minimum Eagle medium (MEM)–α (12000-014, Invitrogen) supplemented with 1% ITS (insulin-transferrin-sodium selenite medium) (I3146, Invitrogen), $NaHCO_3$ (2.1 mg/ml; Sigma-Aldrich), 5% fetal bovine serum (GIBCO, Life Technologies), FSH (1:4000), and penicillin-streptomycin (100 IU/ml; 15140122, Invitrogen) (*57*). The cultured follicles were photographed in a living cell workstation (Okolab) at 37°C, 5% CO_2 by an Andor Dragonfly 502 spinning-disc confocal microscope with following index. In detail, images were acquired by an Andor Dragonfly 502 spinning-disc confocal microscope equipped with a 20× 0.8 NA, a sCMOS camera (Andor Zyla 4.2), and 488-nm (mG) and 568-nm (mT) lines of the Andor ILE system with a spinning-disc confocal scan head (Andor Dragonfly 500). The blood vessels were acquired through Z-step mode with the index. In detail, images were acquired with laser 488-nm around 10 to 20%, laser 568-nm around 15 to 25%, exposure time 100

to 200 ms, and Z-step 0.3 to 0.6 μm for 200 to 250 μm by Fusion 2.1 software (https://andor.oxinst.com/products/dragonfly#fusion). The time-lapse imaging was acquired every 1 hour for 24 continuous hours to trace the change of follicle blood vessels.

Single-follicle transplantation

The follicles of *Tek-Cre;Rainbow* mice were isolated according to the method described above, and then, the isolated follicles were transplanted into the ovaries of wild-type adult females at 6 to 8 weeks of age. In detail, the mice were anesthetized with Avertin (300 mg/kg; T48402, Sigma-Aldrich) (*58*). Next, the ovaries were exposed through the incisions (around 0.5 cm) on the back of animals gently. Then, the fat pad of the ovaries was gently removed, and an approximately 1-mm wound was cut on the ovaries by ophthalmic scissors under the stereoscope. The single follicle was held by an oral pipette to seed into the wound one by one. Around four single follicles were seeded into one incision evenly, and one to three incisions were cut on one ovary to seed and to keep around 4 to 13 exogenous follicles to be transplanted to one RO. In the experiment, a total of 98 recipient females underwent surgery to transplant the exogenous follicles, and the transplanted ovaries were collected after 2 or 4 weeks of surgery to trace the development.

Histological analysis

The ovaries were fixed in 4% (w/v) paraformaldehyde (SC-281692, Santa Cruz) for 12 to 24 hours and then embedded in paraffin (39601095, Leica) after dehydration. Then, the ovaries were serially cut into 8-μm sections with a microtome (RM2245, Leica), and all sections were carefully analyzed under the microscope (DM500, Leica). To count the follicle number, tissue sections were stained with hematoxylin (SC-24973A, Santa Cruz). PFs were counted in every third section and multiplied by three to calculate the number of all PFs in each ovary. Every section was counted for the presence of GFs. The number of PFs and GFs was summed to the total number of follicles.

We studied the effect of inhibiting the vascularization of adult ovaries on the activation rate of PFs by counting the ratio of transient (*59*) follicles. The transient follicles were identified by a mixed flatten and cuboidal GCs of the follicles. The percentage of activated PFs was quantified as the number of transient follicles divided by the total number of PFs in the ovary.

Immunofluorescence and confocal microscopy

Immunostaining was performed according to previously described protocols (*60*). Briefly, the collected ovaries were fixed with 4% (w/v) PFA for 12 to 24 hours, dehydrated, embedded in paraffin, and cut into 8-μm sections. After deparaffinizing and gradually hydrating the sections, they were put into 0.01% sodium citrate buffer (pH 6.0) and then subjected to microwave antigen retrieval for 16 min. The sections were blocked with 10% donkey serum (Jackson ImmunoResearch) at room temperature for 1 hour, and then the tissue sections were incubated with primary antibodies overnight at 4°C. Next, the sections were thoroughly washed in PBS, incubated with the secondary antibody at room temperature for 1 hour, then stained with Hoechst 33342 (B2261, Sigma-Aldrich) for 1 min. The main primary antibodies used in immunofluorescence are as follows: goat anti-FOXL2 (1:300 dilution; IMG-3228, Novus Biologicals) and DDX4 (1:300 dilution; ab27591, Abcam). Second antibody dilution: donkey anti-goat Alexa Fluor 488 (1:150 dilution; A11055, Invitrogen) and donkey anti-rabbit Alexa Fluor 555 (1:150 dilution; A31572, Invitrogen). Images were acquired on a Nikon Eclipse Ti digital fluorescence microscope, Leica (DMi8), or Andor Dragonfly spinning-disc confocal microscope. The image data were analyzed by the software ImageJ. Image merging was by using the color-merge channels function in ImageJ.

Axi treatment

Axi (S1005, Selleck) was dissolved in dimethyl sulfoxide (DMSO; 20688, Thermo Fisher Scientific, USA) and was intraperitoneally injected to the females with a dosage of 30 mg/kg BW every other day. The control mice were injected with the same volume of solvent DMSO in the same way.

For the experiment of blood vessel detection and ovarian reserve analysis, Axi was intraperitoneally injected into 2-month-old wild-type females for 1 month. For the dynamic tracing experiment of GF development, the labeled *Zp3-CreER^{T2};mTmG* females were injected with Axi after 7 days of Tam treatment, and Axi was treated for the entire period of tracing to detect the effect of follicle development after angiogenesis blocking. For the testing of reproductive life span in the long term, Axi was intraperitoneally injected into 7-month-old wild-type females for 1 month. Then, the treated females were mated with adult fertile males to monitor their fertility.

Measurements of serum hormones

The serum hormone levels were determined according to previously described protocols (*61*). To avoid the influence of different estrous cycle stages on the levels of serum hormones, orbital blood was obtained between 8:00 and 10:00 a.m. at diestrus under anesthetized conditions with Avertin (300 mg/kg BW, intraperitoneally). Serum (350 μl) was separated by centrifugation at 3000 rpm at 4°C and stored at −80°C until analysis. Levels of FSH, E2, and P4 were measured using radioimmunoassay kits provided by the Beijing North Institute of Biological Technology (Beijing, China).

Fertility testing

Mating trials were initiated at 1 week after Axi cessation. Healthy males at 8 to 10 weeks of age with proven fertility were used for mating. During the mating experiment, two female mice were placed in a cage with one male for several months (at 18 months of age) until the mice in the control group lost their reproductive capacity. The number of offspring delivered per female was recorded twice per week and was reflected in the reproductive curve. To better evaluate the differential reproductivity between the Axi and control groups, we divided the whole mating weeks according to the mouse age, and the number of delivered pups per female was counted independently at each stage.

Statistical analysis

All experiments were repeated more than three times and showed representative results. The data were presented as means ± SD of each experiment. The data were analyzed by a Student's *t* test and were considered statistically significant at $P < 0.05$. *P* is indicated as follows: $^{*}P < 0.05$, $^{**}P < 0.01$, $^{***}P < 0.001$, and n.s. (not significant, $P \geq 0.05$). Statistics and graphs were obtained using Prism 5 (GraphPad Software, La Jolla). All mice were randomly assigned to different experimental groups. In the process of analyzing experimental results, there was no blind assignment of researchers.

SUPPLEMENTARY MATERIALS

Supplementary material for this article is available at https://science.org/doi/10.1126/sciadv.abi8683

View/request a protocol for this paper from *Bio-protocol*.

REFERENCES AND NOTES

1. A. J. W. Hsueh, K. Kawamura, Y. Cheng, B. C. J. M. Fauser, Intraovarian control of early folliculogenesis. *Endocr. Rev.* **36**, 1–24 (2015).
2. P. Carmeliet, Angiogenesis in life, disease and medicine. *Nature* **438**, 932–936 (2005).
3. Y. H. Cao, Adipose tissue angiogenesis as a therapeutic target for obesity and metabolic diseases. *Nat. Rev. Drug Discov.* **9**, 107–115 (2010).
4. Y. Cao, Angiogenesis and vascular functions in modulation of obesity, adipose metabolism, and insulin sensitivity. *Cell Metab.* **18**, 478–489 (2013).
5. R. S. Robinson, The critical importance of ovarian angiogenesis. *Reprod. Fertil. Dev.* **25**, iii–v (2013).
6. W. Risau, Mechanisms of angiogenesis. *Nature* **386**, 671–674 (1997).
7. S. A. Eming, P. Martin, M. Tomic-Canic, Wound repair and regeneration: Mechanisms, signaling, and translation. *Sci. Transl. Med.* **6**, 265sr6 (2014).
8. S. M. Weis, D. A. Cheresh, Tumor angiogenesis: Molecular pathways and therapeutic targets. *Nat. Med.* **17**, 1359–1370 (2011).
9. Y. Cao, VEGF-targeted cancer therapeutics-paradoxical effects in endocrine organs. *Nat. Rev. Endocrinol.* **10**, 530–539 (2014).
10. T. Shimizu, Y. Hoshino, H. Miyazaki, E. Sato, Angiogenesis and microvasculature in the female reproductive organs: Physiological and pathological implications. *Curr. Pharm. Des.* **18**, 303–309 (2012).
11. Y. Cao, Multifarious functions of PDGFs and PDGFRs in tumor growth and metastasis. *Trends Mol. Med.* **19**, 460–473 (2013).
12. R. K. Jain, Normalizing tumor vasculature with anti-angiogenic therapy: A new paradigm for combination therapy. *Nat. Med.* **7**, 987–989 (2001).
13. B. I. Rini, E. R. Plimack, V. Stus, R. Gafanov, R. Hawkins, D. Nosov, F. Pouliot, B. Alekseev, D. Soulieres, B. Melichar, I. Vynnychenko, A. Kryzhanivska, I. Bondarenko, S. J. Azevedo, D. Borchiellini, C. Szczylik, M. Markus, R. S. McDermott, J. Bedke, S. Tartas, Y. H. Chang, S. Tamada, Q. Shou, R. F. Perini, M. Chen, M. B. Atkins, T. Powles; KEYNOTE-426 Investigators, Pembrolizumab plus axitinib versus sunitinib for advanced renal-cell carcinoma. *N. Engl. J. Med.* **380**, 1116–1127 (2019).
14. Y. Cao, J. Arbiser, R. J. D'Amato, P. A. D'Amore, D. E. Ingber, R. Kerbel, M. Klagsbrun, S. Lim, M. A. Moses, B. Zetter, H. Dvorak, R. Langer, Forty-year journey of angiogenesis translational research. *Sci. Transl. Med.* **3**, 114rv3 (2011).
15. Y. H. Cao, Positive and negative modulation of angiogenesis by VEGFR1 Ligands. *Sci. Signal.* **2**, re1 (2009).
16. L. J. Wilmes, M. G. Pallavicini, L. M. Fleming, J. Gibbs, D. H. Wang, K. L. Li, S. C. Partridge, R. G. Henry, D. R. Shalinsky, D. Hu-Lowe, J. W. Park, T. M. McShane, Y. Lu, R. C. Brasch, N. M. Hylton, AG-013736, a novel inhibitor of VEGF receptor tyrosine kinases, inhibits breast cancer growth and decreases vascular permeability as detected by dynamic contrast-enhanced magnetic resonance imaging. *Magn. Reson. Imaging* **25**, 319–327 (2007).
17. B. I. Rini, B. Escudier, P. Tomczak, A. Kaprin, C. Szczylik, T. E. Hutson, M. D. Michaelson, V. A. Gorbunova, M. E. Gore, I. G. Rusakov, S. Negrier, Y. C. Ou, D. Castellano, H. Y. Lim, H. Uemura, J. Tarazi, D. Cella, C. Chen, B. Rosbrook, S. Kim, R. J. Motzer, Comparative effectiveness of axitinib versus sorafenib in advanced renal cell carcinoma (AXIS): A randomised phase 3 trial. *Lancet* **378**, 1931–1939 (2011).
18. J. Welti, S. Loges, S. Dimmeler, P. Carmeliet, Recent molecular discoveries in angiogenesis and antiangiogenic therapies in cancer. *J. Clin. Invest.* **123**, 3190–3200 (2013).
19. L. P. Reynolds, S. D. Killilea, D. A. Redmer, Angiogenesis in the female reproductive-system. *FASEB J.* **6**, 886–892 (1992).
20. H. M. Fraser, C. Wulff, Angiogenesis in the corpus luteum. *Reprod. Biol. Endocrinol.* **1**, 88 (2003).
21. A. Erturk, K. Becker, N. Jahrling, C. P. Mauch, C. D. Hojer, J. G. Egen, F. Hellal, F. Bradke, M. Sheng, H. U. Dodt, Three-dimensional imaging of solvent-cleared organs using 3DISCO. *Nat. Protoc.* **7**, 1983–1995 (2012).
22. R. Tomer, L. Ye, B. Hsueh, K. Deisseroth, Advanced CLARITY for rapid and high-resolution imaging of intact tissues. *Nat. Protoc.* **9**, 1682–1697 (2014).
23. E. A. Susaki, K. Tainaka, D. Perrin, F. Kishino, T. Tawara, T. M. Watanabe, C. Yokoyama, H. Onoe, M. Eguchi, S. Yamaguchi, T. Abe, H. Kiyonari, Y. Shimizu, A. Miyawaki, H. Yokota, H. R. Ueda, Whole-brain imaging with single-cell resolution using chemical cocktails and computational analysis. *Cell* **157**, 726–739 (2014).
24. W. Z. Li, R. N. Germain, M. Y. Gerner, Multiplex, quantitative cellular analysis in large tissue volumes with clearing-enhanced 3D microscopy (C_e3D). *Proc. Natl. Acad. Sci. U.S.A.* **114**, E7321–E7330 (2017).
25. C. Kirst, S. Skriabine, A. Vieites-Prado, T. Topilko, P. Bertin, G. Gerschenfeld, F. Verny, P. Topilko, N. Michalski, M. Tessier-Lavigne, N. Renier, Mapping the fine-scale organization and plasticity of the brain vasculature. *Cell* **180**, 780–795.e25 (2020).
26. Y. Feng, P. Cui, X. Lu, B. Hsueh, F. Möller Billig, L. Zarnescu Yanez, R. Tomer, D. Boerboom, P. Carmeliet, K. Deisseroth, A. J. W. Hsueh, CLARITY reveals dynamics of ovarian follicular architecture and vasculature in three-dimensions. *Sci. Rep.* **7**, 44810 (2017).
27. J. McKey, L. A. Cameron, D. Lewis, I. S. Batchvarov, B. Capel, Combined iDISCO and CUBIC tissue clearing and lightsheet microscopy for in toto analysis of the adult mouse ovary. *Biol. Reprod.* **102**, 1080–1089 (2020).
28. W. Zheng, H. Zhang, N. Gorre, S. Risal, Y. Shen, K. Liu, Two classes of ovarian primordial follicles exhibit distinct developmental dynamics and physiological functions. *Hum. Mol. Genet.* **23**, 920–928 (2014).
29. H. Zhang, L. Liu, X. Li, K. Busayavalasa, Y. Shen, O. Hovatta, J. A. Gustafsson, K. Liu, Life-long in vivo cell-lineage tracing shows that no oogenesis originates from putative germline stem cells in adult mice. *Proc. Natl. Acad. Sci. U.S.A.* **111**, 17983–17988 (2014).
30. Y. Y. Kisanuki, R. E. Hammer, J. Miyazaki, S. C. Williams, J. A. Richardson, M. Yanagisawa, Tie2-Cre transgenic mice: A new model for endothelial cell-lineage analysis in vivo. *Dev. Biol.* **230**, 230–242 (2001).
31. S. Wiszniak, F. E. Mackenzie, P. Anderson, S. Kabbara, C. Ruhrberg, Q. Schwarz, Neural crest cell-derived VEGF promotes embryonic jaw extension. *Proc. Natl. Acad. Sci. U.S.A.* **112**, 6086–6091 (2015).
32. E. Geva, R. B. Jaffe, Role of vascular endothelial growth factor in ovarian physiology and pathology. *Fertil. Steril.* **74**, 429–438 (2000).
33. M. Hellstrom, L. K. Phng, J. J. Hofmann, E. Wallgard, L. Coultas, P. Lindblom, J. Alva, A. K. Nilsson, L. Karlsson, N. Gaiano, K. Yoon, J. Rossant, M. L. Iruela-Arispe, M. Kalen, H. Gerhardt, C. Betsholtz, Dll4 signalling through Notch1 regulates formation of tip cells during angiogenesis. *Nature* **445**, 776–780 (2007).
34. P. Carmeliet, R. K. Jain, Molecular mechanisms and clinical applications of angiogenesis. *Nature* **473**, 298–307 (2011).
35. M. Potente, H. Gerhardt, P. Carmeliet, Basic and therapeutic aspects of angiogenesis. *Cell* **146**, 873–887 (2011).
36. C. Betz, A. Lenard, H. G. Belting, M. Affolter, Cell behaviors and dynamics during angiogenesis. *Development* **143**, 2249–2260 (2016).
37. A. A. G. Adam, Y. Takahashi, S. Katagiri, M. Nagano, In vitro culture of mouse preantral follicles using membrane inserts and developmental competence of in vitro ovulated oocytes. *J. Reprod. Dev.* **50**, 579–586 (2004).
38. H. Zhang, W. J. Zheng, Y. Shen, D. Adhikari, H. Ueno, K. Liu, Experimental evidence showing that no mitotically active female germline progenitors exist in postnatal mouse ovaries. *Proc. Natl. Acad. Sci. U.S.A.* **109**, 12580–12585 (2012).
39. C. Wulff, S. J. Wiegand, P. T. Saunders, G. A. Scobie, H. M. Fraser, Angiogenesis during follicular development in the primate and its inhibition by treatment with truncated Flt-1-Fc (vascular endothelial growth factor Trap(A40)). *Endocrinology* **142**, 3244–3254 (2001).
40. H. M. Fraser, Regulation of the ovarian follicular vasculature. *Reprod. Biol. Endocrinol.* **4**, 18 (2006).
41. R. S. Robinson, K. J. Woad, A. J. Hammond, M. Laird, M. G. Hunter, G. E. Mann, Angiogenesis and vascular function in the ovary. *Reproduction* **138**, 869–881 (2009).
42. H. Zhang, K. Liu, Cellular and molecular regulation of the activation of mammalian primordial follicles: Somatic cells initiate follicle activation in adulthood. *Hum. Reprod. Update* **21**, 779–786 (2015).
43. M. J. Bertoldo, D. R. Listijono, W.-H. J. Ho, A. H. Riepsamen, D. M. Goss, D. Richani, X. L. Jin, S. Mahbub, J. M. Campbell, A. Habibalahi, W.-G. N. Loh, N. A. Youngson, J. Maniam, A. S. A. Wong, K. Selesniemi, S. Bustamante, C. Li, Y. Q. Zhao, M. B. Marinova, L.-J. Kim, L. Lau, R. M. Wu, A. S. Mikolaizak, T. Araki, D. G. Le Couteur, N. Turner, M. J. Morris, K. A. Walters, E. Goldys, C. O'Neill, R. B. Gilchrist, D. A. Sinclair, H. A. Homer, L. E. Wu, NAD^+ repletion rescues female fertility during reproductive aging. *Cell Rep.* **30**, 1670–1681.e7 (2020).
44. Y. Miao, Z. Cui, Q. Gao, R. Rui, B. Xiong, Nicotinamide mononucleotide supplementation reverses the declining quality of maternally aged oocytes. *Cell Rep.* **32**, 107987 (2020).
45. W. M. Amselgruber, M. Schafer, F. Sinowatz, Angiogenesis in the bovine corpus luteum: An immunocytochemical and ultrastructural study. *Anat. Histol. Embryol.* **28**, 157–166 (1999).
46. M. Boareto, M. K. Jolly, E. Ben-Jacob, J. N. Onuchic, Jagged mediates differences in normal and tumor angiogenesis by affecting tip-stalk fate decision. *Proc. Natl. Acad. Sci. U.S.A.* **112**, E3836–E3844 (2015).
47. T. Kangsamaksin, A. Murtomaki, N. M. Kofler, H. Cuervo, R. A. Chaudhri, I. W. Tattersall, P. E. Rosenstiel, C. J. Shawber, J. Kitajewski, NOTCH decoys that selectively block DLL/NOTCH or JAG/NOTCH disrupt angiogenesis by unique mechanisms to inhibit tumor growth. *Cancer Discov.* **5**, 182–197 (2015).
48. B. Berisha, D. Schams, D. Rodler, M. W. Pfaffl, Angiogenesis in the ovary - the most important regulatory event for follicle and corpus luteum development and function in cow - an overview. *Anat. Histol. Embryol.* **45**, 124–130 (2016).

49. F. J. Broekmans, M. R. Soules, B. C. Fauser, Ovarian aging: Mechanisms and clinical consequences. *Endocr. Rev.* **30**, 465–493 (2009).
50. Q. Li, X. D. Geng, W. Zheng, J. Tang, B. Xu, Q. H. Shi, Current understanding of ovarian aging. *Sci. China Life Sci.* **55**, 659–669 (2012).
51. H. Buckler, The menopause transition: Endocrine changes and clinical symptoms. *J. Br. Menopause Soc.* **11**, 61–65 (2005).
52. P. Monteleone, G. Mascagni, A. Giannini, A. R. Genazzani, T. Simoncini, Symptoms of menopause - global prevalence, physiology and implications. *Nat. Rev. Endocrinol.* **14**, 199–215 (2018).
53. R. C. Zimmermann, E. Xiao, N. Husami, M. V. Sauer, R. Lobo, J. Kitajewski, M. Ferin, Short-term administration of antivascular endothelial growth factor antibody in the late follicular phase delays follicular development in the rhesus monkey. *J. Clin. Endocrinol. Metab.* **86**, 768–772 (2001).
54. R. Constien, A. Forde, B. Liliensiek, H. J. Grone, P. Nawroth, G. Hammerling, B. Arnold, Characterization of a novel EGFP reporter mouse to monitor Cre recombination as demonstrated by a Tie2 Cre mouse line. *Genesis* **30**, 36–44 (2001).
55. W. J. de Lange, C. M. Halabi, A. M. Beyer, C. D. Sigmund, Germ line activation of the Tie2 and SMMHC promoters causes noncell-specific deletion of floxed alleles. *Physiol. Genomics* **35**, 1–4 (2008).
56. X. Tian, T. Hu, H. Zhang, L. He, X. Huang, Q. Liu, W. Yu, L. He, Z. Yang, Z. Zhang, T. P. Zhong, X. Yang, Z. Yang, Y. Yan, A. Baldini, Y. Sun, J. Lu, R. J. Schwartz, S. M. Evans, A. C. Gittenberger-de Groot, K. Red-Horse, B. Zhou, Subepicardial endothelial cells invade the embryonic ventricle wall to form coronary arteries. *Cell Res.* **23**, 1075–1090 (2013).
57. L. J. Green, A. Shikanov, In vitro culture methods of preantral follicles. *Theriogenology* **86**, 229–238 (2016).
58. L. M. Hablitz, H. S. Vinitsky, Q. Sun, F. F. Staeger, B. Sigurdsson, K. N. Mortensen, T. O. Lilius, M. Nedergaard, Increased glymphatic influx is correlated with high EEG delta power and low heart rate in mice under anesthesia. *Sci. Adv.* **5**, eaav5447 (2019).
59. J. P. de Bruin, M. Dorland, E. R. Spek, G. Posthuma, M. van Haaften, C. W. N. Looman, E. R. te Velde, Age-related changes in the ultrastructure of the resting follicle pool in human ovaries. *Biol. Reprod.* **70**, 419–424 (2004).
60. L. Feng, Y. Wang, H. Cai, G. Sun, W. Niu, Q. Xin, X. Tang, J. Zhang, C. Wang, H. Zhang, G. Xia, ADAM10-Notch signaling governs the recruitment of ovarian pregranulosa cells and controls folliculogenesis in mice. *J. Cell Sci.* **129**, 2202–2212 (2016).
61. X. Dou, Y. Sun, J. Li, J. Zhang, D. Hao, W. Liu, R. Wu, F. Kong, X. Peng, J. Li, Short-term rapamycin treatment increases ovarian lifespan in young and middle-aged female mice. *Aging Cell* **16**, 825–836 (2017).

Acknowledgments: We thank H. Chen (College of Life Sciences, Nanjing Normal University, China) for sharing the *Tek-Cre* mouse line and K. Liu (Department of Obstetrics and Gynecology, The University of Hong Kong, Hong Kong, China.) for sharing the *Rainbow* mouse line. We are also grateful to X. Xu for drawing the illustrations in the manuscript. **Funding:** This study was supported by the National Key Research and Development Program of China to Y.Z. and H.Z. (2018YFC1003700 and 2017YFC1001100) and the National Natural Science Foundation of China (81873815 and 31571542). **Author contributions:** X.X., Y.Z., and H.Z. designed the research; X.X., L.M., L.L., J.L., S.Z., L.J., X.Y., Y.D., J.Z., Y.W., and S.N. performed the experiments; X.X., G.X., Y.Y., Y.Z., Y.C., and H.Z. analyzed the data; X.X. and H.Z. wrote the paper. All authors have seen and approved the final version. **Competing interests:** The authors declare that they have no competing interests. **Data and materials availability:** All data needed to evaluate the conclusions in the paper are present in the paper and the Supplementary Materials.

Submitted 6 April 2021
Accepted 18 November 2021
Published 12 January 2022
10.1126/sciadv.abi8683

ScienceAdvances

Imaging and tracing the pattern of adult ovarian angiogenesis implies a strategy against female reproductive aging

Xueqiang XuLu MuLingyu LiJing LiangShuo ZhangLongzhong JiaXuebing YangYanli DaiJiawei ZhangYibo WangShudong NiuGuoliang XiaYunlong YangYan ZhangYihai CaoHua Zhang

Sci. Adv., 8 (2), eabi8683. • DOI: 10.1126/sciadv.abi8683

Science Advances (ISSN) is published by the American Association for the Advancement of Science. 1200 New York Avenue NW, Washington, DC 20005. The title *Science Advances* is a registered trademark of AAAS.